CMS Physics Analysis Summary

Contact: cms-pag-conveners-higgs@cern.ch 2018/07/05

Search for the associated production of a Higgs boson and a single top quark in pp collisions at $\sqrt{s} = 13\,\text{TeV}$

The CMS Collaboration

Abstract

A search for the production of Higgs boson in association with a single top quark is presented, based on data collected in 2016 with the CMS detector at the LHC at a center of mass energy of 13 TeV, which corresponds to an integrated luminosity of 35.9 fb^{-1}. The production cross section of this process is highly sensitive to the absolute values of the modifiers of the top quark-Higgs boson coupling, κ_t, and the coupling of vector bosons to the Higgs boson, κ_V, as well as their relative signs with respect to the standard model. Analyses using multilepton signatures due to $\text{H} \to \text{WW}$, $\text{H} \to \tau\tau$, and $\text{H} \to \text{ZZ}$ decay modes and that with a single lepton for the decay $\text{H} \to \text{b}\bar{\text{b}}$ are combined with a reinterpretation of a measurement of $\text{H} \to \gamma\gamma$ to constrain κ_t. For $\kappa_\text{V} = 1.0$ the observed data favor positive values of κ_t and exclude values of κ_t below about 0.9.

1 Introduction

The scalar resonance discovered by the CMS and ATLAS Collaborations at the LHC [1–3] in 2012 has been found to be consistent with the predictions of the standard model (SM) for a Higgs boson of mass 125.09 GeV [4]. In particular, its couplings to fermions have been found to be proportional to their masses and it is observed to have zero spin and positive parity [5]. Recently, the associated production of top quark pairs with a Higgs boson ($t\bar{t}H$) has been observed [6, 7], thereby directly probing the Yukawa interaction between Higgs bosons and top quarks. In addition to measuring the absolute strengths of Higgs couplings it is important to assess the possible existence of relative phases among the couplings and their general Lorentz structure. A broad sweep of possible Higgs production mechanisms and decay modes must be considered to reveal possible deviations from the SM expectations.

Most probes of the top quark-Higgs boson interaction are either sensitive only to the magnitude of the top-Higgs Yukawa coupling y_t, such as measurements of $t\bar{t}H$ [6, 7] production, or must rely on indirect effects from loop interactions, such as studies using Higgs decays to photon pairs [8] or the associated production of Higgs and Z bosons via gluon-gluon fusion [9]. The resulting constraints on the coupling rely on the assumption of only SM particles in the loops [10]. Further, such measurements currently disfavor a negative value of the coupling, without excluding it [11, 12].

In contrast, the production of Higgs bosons in association with single top quarks in pp collisions proceeds via two dominant leading-order diagrams [13–16] and due to the interference effects, is uniquely sensitive to both the magnitude as well as the sign of the coupling. Representative diagrams for the *t*-channel production process (tHq) are shown in Fig. 1. In

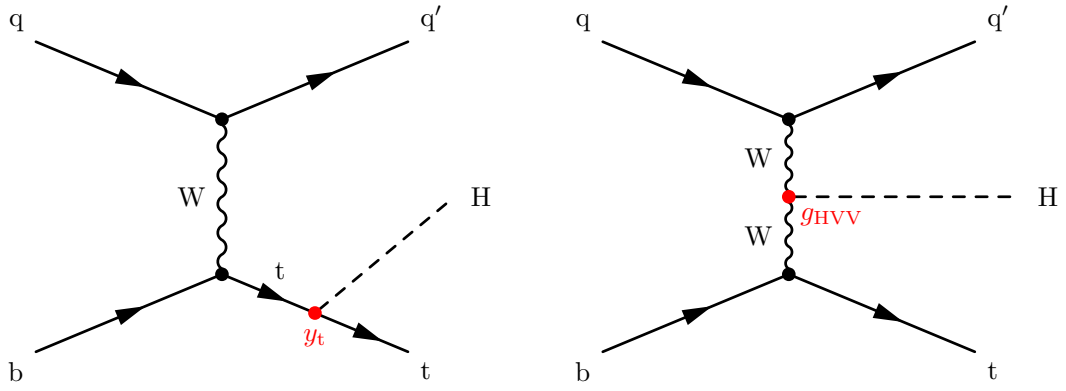

Figure 1: Leading-order Feynman diagrams for the associated production of single top quark and Higgs boson in the *t*-channel where the Higgs boson couple either to the top quark or the W boson.

the SM, the interference is destructive and leads to very small production cross sections of 70.96 fb, 2.86 fb, and 15.61 fb for the *t*, *s*, and tW processes, respectively at center-of-mass energy $\sqrt{s} = 13$ TeV [17]. Hence the data collected at LHC so far is not yet sensitive to the SM process. However, in the presence of new physics, a non-SM like relative sign between the t-H and W-H couplings can lead to constructive interference and the cross sections are enhanced by about one order of magnitude, thereby exceeding those for $t\bar{t}H$ production and rendering tHq production accessible with current LHC datasets. In this paper, the tHq and tHW processes have been collectively referred to as tH production, while neglecting *s*-channel production, since it has vanishingly small cross section.

The event topology of tHq production is that of two heavy objects—the top quark, and the

Higgs boson—in the central portion of the detector recoiling against one another, while a light quark and a soft b quark escape in the forward-backward regions of the detector. Leptonic top quark decays produce high momentum electrons and muons that can be used to trigger the detector. Higgs boson decays to vector bosons or τ leptons ($H \to WW^*$, ZZ^*, or $\tau\tau$) lead to a multilepton final state with comparatively low background contributions from other processes. Higgs boson decays to bottom quark-antiquark pairs ($H \to b\bar{b}$), on the other hand, provide a larger event rate albeit with challenging backgrounds from $t\bar{t}$+jets production. In contrast, Higgs boson decays to two photons ($H \to \gamma\gamma$) result in easy-to-trigger and relatively clean signals for both leptonic or fully hadronic top quark decays, with backgrounds mainly from other production modes of Higgs boson. The production of tHW lacks the presence of forward activity and involves three heavy objects and therefore lacks the defining features of tHq events, while closely resembling the $t\bar{t}H$ topologies.

The CMS Collaboration has previously searched for anomalous tH production at $\sqrt{s} = 8\,\text{TeV}$, assuming inverted couplings: $y_t = -y_t^{SM}$, using all the relevant Higgs boson decay modes, and set limits on the cross section [18]. In the second running period of the LHC at 13 TeV center of mass energy, two dedicated analyses are searching for tH production in multilepton channels and in the $H \to b\bar{b}$ channel [19, 20], using CMS data. This documents reports the result of their combination, together with the reinterpretation of a previous result in the $\gamma\gamma$ channel [21].

2 CMS Experiment

The central feature of the CMS apparatus is a superconducting solenoid of 6 m internal diameter, providing a magnetic field of 3.8 T along the beam direction. Within the solenoid volume are a silicon pixel and strip tracker, a lead tungstate crystal electromagnetic calorimeter (ECAL), and a brass and scintillator hadron calorimeter (HCAL), each composed of a barrel and two endcap sections providing pseudorapidity coverage up to $|\eta| < 3.0$. Forward calorimeters employing cherenkov light detection extend the acceptance to $|\eta| < 5.0$. Muons are detected in gas-ionization chambers embedded in the steel flux-return yoke outside the solenoid with a fiducial of $|\eta| < 2.4$. The silicon tracker system measures charged particles within the pseudorapidity range $|\eta| < 2.5$. The impact parameter in the transverse (longitudinal) directions are measured with an uncertainty of 10 (30) μm respectively [22]. Tracks of isolated muons of transverse momentum $p_T \geq 100\,\text{GeV}$ and $|\eta| < 1.4$ are reconstructed with an efficiency close to 100% and a p_T resolution of about 1.3 to 2% and better than 6% for higher values of η. For $p_T \leq 1\,\text{TeV}$ the resolution in the central region is better than 10%. A two-level trigger system is used to reduce the rate of recorded events to a level suitable for data acquisition and storage. The first level of the CMS trigger system, composed of custom hardware processors, uses information from the calorimeters and muon detectors to select the most interesting events in a time interval of less than 4 μs. The high-level trigger processor farm further decreases the event rate from around 100 kHz to about 1 kHz. A more detailed description of the CMS detector, together with a definition of the coordinate system and the kinematic variables used in the analysis, can be found in Ref. [23].

A full event reconstruction is performed by the particle-flow (PF) algorithm using the optimized and combined information from all the sub-detectors [24]. The individual PF candidates reconstructed are muons, electrons, photons, and charged and neutral hadrons, which are then used to reconstruct higher-level objects such as jets, hadronic taus, and missing transverse energy. Additional quality criteria are applied to the objects to improve the selection purity.

Collision vertices are reconstructed using a deterministic annealing algorithm [25, 26]. The reconstructed vertex position is required to be compatible with the location of the LHC beam

in the x-y plane. The vertex with the largest value of summed physics-object p_T^2 is considered to be the primary pp interaction (PV). Charged particles which are subsequently reconstructed are required to be compatible with originating from the selected PV.

Electrons are reconstructed using an algorithm that matches tracks reconstructed in the silicon tracker to energy deposits in the ECAL, without any deposits in HCAL [27]. A dedicated algorithm takes into account the emission of bremsstrahlung photons and determines the energy loss.A multivariate analysis (MVA) approach based on boosted decision trees (BDT) is employed to distinguish electrons from hadrons mimicking an electron signature. This electron identification BDT has been trained on samples of electrons and hadrons. Additional requirements are applied in order to remove electrons originating from photon conversions [27].

The identification of muons is based on linking track segments reconstructed in the silicon tracking detector and in the muon system [28]. If a link can be established, the track parameters are recomputed using the combination of hits in the inner and outer detectors. Quality requirements are applied on the multiplicity of hits in the track segments, on the number of matched track segments and on the quality of the track fit [28].

Jets are reconstructed from charged and neutral PF candidates using the anti-k_T algorithm [29, 30] with a distance parameter of 0.4, and with the constraint that the charged particles are compatible with the selected PV. Jets originating from the hadronization of b quarks are identified using the "combined secondary vertex" algorithm [31, 32] which exploits observables related to the long lifetime of b hadrons and to the higher particle multiplicity and mass of b jets compared to light-quark and gluon jets.

3 Data and Simulation

Collision events for this analysis are selected by high-level trigger algorithms [33]. Events in the multilepton channels must pass any one of single lepton, dilepton, or trilepton triggers with loose identification and isolation requirements with a minimum p_T threshold, based on the lepton multiplicity in the final state. Events in the $b\bar{b}$ channels must pass the same single lepton triggers, or a dilepton trigger for the control region described in Section 5. The p_T thresholds on leptons applied offline depend on the trigger requirements.

The data are compared to signal and background estimations based on Monte Carlo (MC) simulated samples and data-driven techniques. All simulated samples include the response of the CMS detector based on the GEANT4 [34] package. The event generator used for the tHq and tHW signal samples is MG5_aMC@NLO (version 5.222) [35] at leading-order precision and using the NNPDF3.0 PDF set [36]. The samples are normalized to next-to-leading order (NLO) SM cross sections at 13 TeV of 70.96 fb and 15.61 fb for tHq and tHW, respectively [17].

The Higgs boson production cross sections and branching ratios are expressed as functions of Higgs boson coupling modifiers in the kappa framework [37], where the coupling modifiers κ are defined as the ratio of the actual value of a given coupling to the one predicted by the SM. Particularly relevant for the tH case are the top quark and vector boson coupling modifiers: $\kappa_t \equiv y_t/y_t^{SM}$ and $\kappa_V \equiv g_{HVV}/g_{HVV}^{SM}$, where V stands for both W or Z bosons. The dependence of the tHq and tHW production cross sections on κ_t and κ_V are assumed to be as follows [17]:

$$\sigma_{tHq} = (2.633\,\kappa_t^2 + 3.578\,\kappa_V^2 - 5.211\,\kappa_t\kappa_V) \times \sigma_{tHq}^{SM}$$
$$\sigma_{tHW} = (2.909\,\kappa_t^2 + 2.310\,\kappa_V^2 - 4.220\,\kappa_t\kappa_V) \times \sigma_{tHW}^{SM}.$$

Event weights are produced in the generation of both samples corresponding to 33 values of κ_t

between -6.0 and $+6.0$, and for $\kappa_V = 1.0$. The tHq events are generated with the four-flavor scheme while the tHW process uses the five-flavor scheme to disentangle the leading-order interference with the $t\bar{t}H$ process [38].

MG5_aMC@NLO is also used for the $t\bar{t}H$ process and the main backgrounds: $t\bar{t}W^{\pm}$, $t\bar{t}Z$, $t\bar{t}$+jets, and $t\bar{t}\gamma$ + jets; the rates are normalized to NLO cross sections, where available. In particular, the $t\bar{t}H$ production cross section is 0.507 pb [17]. A set of minor backgrounds are also simulated with MG5_aMC@NLO at leading order, or with different generators, such as POWHEG [39–44]. All generated events are interfaced to PYTHIA8 (v8.205) [45] for the parton shower and hadronization steps.

The object reconstruction in MC follows the same algorithm as used in data. Furthermore, the trigger selection is simulated and applied for generated signal events. However, the triggering and selection efficiencies for leptons are different between data and MC. This is corrected for in simulation using scale factors to improve the modeling of the data.

Each MC sample contains information on additional pp interactions in the same and nearby bunch crossings (pileup). Simulated events are weighted according to the number of pileup interactions so that the distribution of additional interactions in the simulated samples matches that observed in data, as estimated from the measured bunch-to-bunch instantaneous luminosity and the total inelastic cross section, 69.2 mb.

4 Multilepton Channels

The multilepton analysis described in Ref. [19] is an extension of the search for $t\bar{t}H$ in multilepton channels [46], reusing the object selections and background estimation techniques developed for that search.

tH events where the top quark decay produces leptons and the Higgs boson decays to vector bosons or τ leptons can lead to final states containing multiple high-p_T leptons with different charge and flavor configurations. Of particular interest are those with three or more charged leptons or with two leptons of the same electric charge, as they appear with comparatively low backgrounds. Selecting such events in pp collisions while requiring the presence of b-tagged jets typically yields a mixture of mostly $t\bar{t}$+jets events with non-prompt leptons and events from associated production of $t\bar{t}$ with a vector boson, $t\bar{t}V$ ($t\bar{t}W^{\pm}$ and $t\bar{t}Z$), or with a Higgs boson ($t\bar{t}H$) that decay to additional prompt leptons.

Leptons were selected in this analysis using a dedicated multivariate discriminator trained to separate prompt from non-prompt leptons by exploiting the properties of the jet associated with individual leptons in addition to the lepton kinematics and reconstruction quality. The leptons were selected if they passed a certain threshold of the classifier output and are referred to as "tight" leptons. Leptons without any criteria on the classifier output are referred to as "loose" leptons.

The final event selection targets signatures with $H \to WW$ and $t \to Wb \to \ell\nu b$, which results in three W bosons, one b quark, and a light quark at high rapidity. Three mutually exclusive channels were defined based on the number of tight leptons and their flavors: exactly two same sign leptons, either $\mu\mu$ or eμ, and exactly three leptons ($\ell\ell\ell$). A possible dielectron channel suffers from larger backgrounds and does not add sensitivity. In all channels there is the additional requirement of at least one b-tagged jet and at least one light (untagged) jet. The full selection is summarized in Tab. 1.

Table 1: Summary of event selection for the multilepton channels.

Same-sign channel ($\mu\mu$/eμ)	$\ell\ell\ell$ **channel**
Exactly two tight same sign leptons	Exactly three tight leptons
$p_T > 25/15\,\text{GeV}$	$p_T > 25/15/15\,\text{GeV}$
	No lepton pair with $\lvert m_{\ell\ell} - m_Z \rvert < 15\,\text{GeV}$
No loose leptons with $m_{\ell\ell} < 12\,\text{GeV}$	
One or more b tagged jet with $p_T > 25\,\text{GeV}$ and $\lvert\eta\rvert < 2.4$	
One or more untagged jet with $p_T > 25\,\text{GeV}$ for $\lvert\eta\rvert < 2.4$ and $p_T > 40\,\text{GeV}$ for $\lvert\eta\rvert > 2.4$	

Irreducible backgrounds such as $t\bar{t}V$ give rise to final states very similar to the tHq signal and were directly estimated from MC simulation, while applying data-to-MC correction factors. The dominant contributions from reducible backgrounds arising from non-prompt leptons (mainly $t\bar{t}$ production) were estimated using sidebands in the data with looser lepton selections and measuring a loose-to-tight extrapolation in a background-dominated control selection.

To discriminate the small signal from the backgrounds, a multivariate method was employed: a classification algorithm was trained twice with tHq events (but not tHW or $t\bar{t}H$ events) as the signal class, and either $t\bar{t}V$ (mixing $t\bar{t}W^{\pm}$ and $t\bar{t}Z$ according to their respective cross sections) or $t\bar{t}$+jets as background classes. The algorithm takes advantage of distinguishing features of the signal and background processes such as the forward light jet, the difference in jet and b tag multiplicities, and the kinematic properties of the leptons. Events from tHW and $t\bar{t}H$ production were not used in the training and, due to their close kinematic similarity with the $t\bar{t}V$ background, tended to be classified as backgrounds.

The events were then sorted into ten categories depending on the output of the two BDT classifiers according to an optimized binning strategy, resulting in a one-dimensional histogram with ten bins which was then fit to the observed data.

The systematic uncertainties with the largest impact on the final result were found to be those related to the normalization of the non-prompt backgrounds, the renormalization and factorization scale variations for the $t\bar{t}V$ and $t\bar{t}H$ processes, and the lepton selection efficiencies.

5 $b\bar{b}$ Channels

The analysis targeting tH with $H \to b\bar{b}$ final states builds on a corresponding search for $t\bar{t}H$ [47], similar to the multilepton analysis summarized in the previous section. The analysis used two selections targeting signal events, with either three or four b tagged jets, and a separate sample with opposite sign dileptons, dominated by $t\bar{t}$+jets events, to control $t\bar{t}$ + heavy flavor ($t\bar{t}$ + HF) events in a simultaneous fit. Multivariate classification algorithms were trained to assign reconstructed jets to partons and to separate the tH signal from the dominant $t\bar{t}$+jets backgrounds. An additional algorithm was trained to separate the different $t\bar{t}$+jets background components in the control region.

Events in the $b\bar{b}$ signal channels were collected using a single lepton trigger, targeting leptonic decays of the top quark. Each event was required to contain exactly one lepton (muon or electron) while rejecting events with additional leptons with $p_T > 15\,\text{GeV}$. A minimal amount of missing transverse momentum of $E_T^{\text{miss}} > 35\,\text{GeV}$ in the muon channel and $E_T^{\text{miss}} > 45\,\text{GeV}$ the electron channel was required to account for the neutrino.

A dilepton control region was defined to constrain the composition of the main background contribution from top quark pair production, requiring exactly two oppositely charged leptons,

two b-tagged jets, and at least one additional jet passing a less strict b tagging requirement. Each event was required to have a minimal amount of missing transverse momentum. The selection criteria are summarized in Table 2.

Table 2: Summary of event selection for analysis with single lepton.

Signal region	**Control region**
One muon (electron) with $p_T > 27(35)$ GeV	Two leptons: $p_T > 20/20$ GeV ($\mu\mu/e\mu$) or $p_T > 20/15$ GeV ($ee/\mu e$)
No additional loose leptons	No additional loose leptons
Three or four b tagged jets $p_T > 30$ GeV and $\|\eta\| < 2.4$	Two b tagged jets $p_T > 30$ GeV and $\|\eta\| < 2.4$
One or more untagged jets $p_T > 30$ GeV for $\|\eta\| < 2.4$ or $p_T > 40$ GeV for $\|\eta\| \geq 2.4$	One or more loose b tagged jets $p_T > 30$ GeV and $\|\eta\| < 2.4$
$E_T^{miss} > 35(45)$ GeV for muons (electrons)	$E_T^{miss} > 40$ GeV

The main backgrounds in the $b\bar{b}$ channel arise from $t\bar{t}$ production with additional jets and were estimated using samples of simulated events. The $t\bar{t}$+jets process was separated into five exclusive categories at the generator level ($t\bar{t} + b\bar{b}$, $t\bar{t} + 2b$, $t\bar{t} + b$, $t\bar{t} + c\bar{c}$, and $t\bar{t} + LF$) and modeled with separate systematic uncertainties in the fit. The dilepton control region was specifically designed to separate and constrain the $t\bar{t} + HF$ and $t\bar{t}$ + light flavor ($t\bar{t} + LF$) components.

The dominant systematic uncertainties of the analysis were found to be from the factorization and renormalization scales, as well as from the overall normalization of the $t\bar{t} + HF$ processes and the uncertainty in the jet energy corrections.

6 Reinterpretation of $H \to \gamma\gamma$

The standard model tHq and tHW signal processes with $H \to \gamma\gamma$ were included in previous measurements of the Higgs boson properties in the diphoton final state [21]. Events with two prompt high-p_T photons were divided into different event categories, each enriched with a particular production mechanism of the Higgs boson. The tHq and tHW processes contribute mostly to the "$t\bar{t}H$ Hadronic", and "$t\bar{t}H$ Leptonic" categories as defined in Ref. [21], which target the $t\bar{t}H$ process for fully hadronic top quark decays and for single or dilepton decay modes, respectively. Events in the $t\bar{t}H$ Leptonic category are selected to have at least one lepton well separated from the photons, and well reconstructed, as well as at least two jets of which at least one passes a b tagging requirement. The $t\bar{t}H$ Hadronic category is defined as events with zero (identically selected) leptons and at least three jets, of which at least one is b tagged.

The signal is modeled with a sum of Gaussian functions describing the diphoton invariant mass ($m_{\gamma\gamma}$) shape derived from simulation. The background contribution is determined from the data without use of simulated events, using the discrete profiling method [4, 48, 49]. Different classes of models describing the falling $m_{\gamma\gamma}$ distribution in the background processes are used as input to the method. Sources of systematic uncertainties affecting the signal model and leading to migrations of signal events among the categories are considered.

The inputs to Ref. [21] from the $t\bar{t}H$ categories are used here in a combination with the multi-lepton and $b\bar{b}$ channels to put constraints on the coupling modifier κ_t and on the production cross section of tH events. The modifiers κ_t and κ_V affect both the tH and $t\bar{t}H$ production cross sections as well as the Higgs boson decay branching ratio into two photons through the in-

terference of boson and fermion loops. Changes in the kinematic properties of the tH signal arising from the modified couplings are taken into account by considering their effect on the signal acceptance and selection efficiency. Figure 2 shows the modified tHq and tHW selection efficiencies including acceptances for those categories as a function of the ratio of coupling modifiers κ_t/κ_V. The signal diphoton shape is found to be independent of κ_t/κ_V.

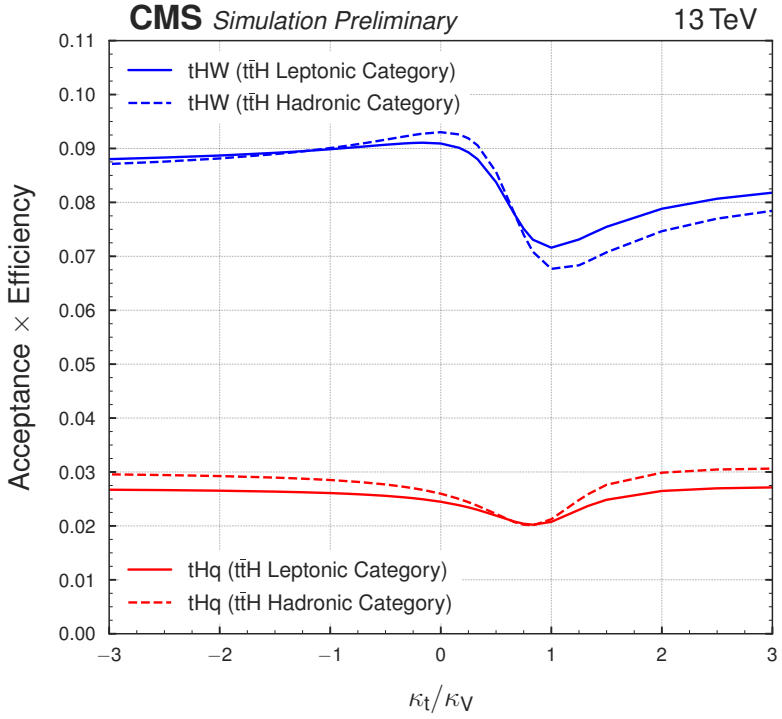

Figure 2: Acceptance and selection efficiency for the tHq (red) and tHW (blue) signal processes as a function of κ_t/κ_V, for the $t\bar{t}H$ Leptonic (solid lines) and $t\bar{t}H$ Hadronic categories (dashed lines).

The dependence of the signal acceptance and efficiency on κ_t/κ_V is implemented in the same statistical framework as that of Ref. [21], modifying the signal only in the $t\bar{t}H$ categories.

7 Combination of Channels

The different discriminator output distributions in the multilepton and $b\bar{b}$ channels and the $\gamma\gamma$ invariant mass in the diphoton channel are compared to the observed data in a combined maximum likelihood fit for the various different assumptions on the signal kinematics and normalizations, and are used to derive constraints on the signal yields.

The event selections in the different channels are mutually exclusive, therefore allowing a straightforward combination. Common systematic uncertainties such as the luminosity normalization, the b tagging uncertainties, and the theoretical uncertainties related to the signal modeling are taken to be fully correlated between the different channels.

A profile likelihood scan is performed as a function of the coupling modifier κ_t, which affects the production cross sections of the three signal components tHq, tHW, and $t\bar{t}H$, as well as the Higgs boson branching fractions. The total Higgs boson decay width is assumed to be fixed at its SM value, i.e. effects on Higgs boson decays via fermion and boson loops to $\gamma\gamma$, $Z\gamma$, and gluon-gluon final states also affect the relative branching ratios in other channels. Furthermore,

the kinematic properties of the two tH processes and thereby the shape of the classifier outputs entering the fit depend on the value of κ_t. Systematic uncertainties are included in the form of nuisance parameters in the fit. Pre-fit systematic uncertainties of the same groups are shown for comparison.

To derive constraints on κ_t for a fixed value of $\kappa_V = 1.0$, a scan of the likelihood ratio $\mathcal{L}(\kappa_t)/\mathcal{L}(\hat{\kappa_t})$ is performed, where $\hat{\kappa_t}$ is the best-fit value of κ_t. Figure 3 shows the negative of twice the logarithm of this likelihood ratio ($-2\Delta \ln(\mathcal{L})$), for scans on the observed data, and for an Asimov dataset with SM expectations for $t\bar{t}H$ and tH. On this scale, a 95% confidence interval covers values below 3.84, while standard deviations are at values of 1, 4, 9, 16, etc. The expected performance for a SM-like signal is to favor a value of $\kappa_t = 1.0$ over one of $\kappa_t = -1.0$ by more than four standard deviations, and to exclude values outside of about -0.5 and 1.6 at 95% confidence level (C.L.). In the combined scan, the observed data slightly favors a positive value of κ_t over a negative one, by about 1.5 standard deviations, while excluding values outside the ranges of about $[-0.9, -0.5]$ and $[1.0, 2.1]$ at 95% C.L. The sensitivity is driven by the $\gamma\gamma$ channel at negative values of the coupling modifiers and by the multilepton channels at positive values.

An excess of observed over expected events is seen both in the multilepton and $\gamma\gamma$ channels, with a combined significance of about two standard deviations. Consequently, the best-fit signal strength under the SM hypothesis is 1.99 ± 0.53. These results are in agreement with those from the dedicated $t\bar{t}H$ searches [6], as expected, since they share a large fraction of events with the dataset used here.

To establish the limits on tH production, a common signal strength parameter for the sum of tHq and tHW is introduced, defined as the ratio of the fitted signal cross section to the SM expectation. A profile likelihood fit for this signal strength is then performed at fixed points of κ_t, and upper limits on the tH production cross section times the combined Higgs boson branching ratios to $WW^* + \tau\tau + ZZ^* + b\bar{b} + \gamma\gamma$ are derived, as shown in Fig. 4. Limits for the SM and for a scenario with $\kappa_t = -1.0$ for the individual channels are shown in Tab. 3. The $t\bar{t}H$ contribution is kept fixed to its κ_t-dependent expectation. The fiducial cross section for SM-like tH production is limited to about 2.0 pb, with an expected limit of 0.9 pb, corresponding, respectively, to about 26 and 12 times the expected cross section times BR. The significant discrepancy of observed and expected limit around $\kappa_t = 0.0$ is caused by the fact that the predicted $t\bar{t}H$ cross section vanishes while the data favors larger than expected yields for $t\bar{t}H$ in both the $\gamma\gamma$ and multilepton channels. This is compatible with the observed and expected limits at the SM value of κ_t.

8 Conclusion

Events in pp collisions at $\sqrt{s} = 13$ TeV compatible with the production of Higgs bosons in association with a single top quark have been studied to derive constraints on the magnitude and relative sign of Higgs boson couplings to top quarks and vector bosons. Dedicated analyses in multilepton and $b\bar{b}$ final states are combined with a reinterpretation of a $H \to \gamma\gamma$ measurement for the final result. For standard model-like Higgs couplings to vector bosons, the observed data favor a positive value of the modifier of the Higgs-top coupling, κ_t by about 1.5 standard deviations and exclude values outside the ranges of about $[-0.9, -0.5]$ and $[1.0, 2.1]$ at 95% C.L. An excess of observed data events over non-Higgs boson backgrounds is compatible with the SM expectation of $tH + t\bar{t}H$ production within about two standard deviations.

Table 3: Expected and observed 95% C.L. upper limits on the tH production cross section times $H \to WW^* + \tau\tau + ZZ^* + b\bar{b} + \gamma\gamma$ branching ratio for a scenario of inverted couplings ($\kappa_t/\kappa_V = -1.0$, top rows) and for a standard model-like signal ($\kappa_t/\kappa_V = 1.0$, bottom rows), in pb. The expected limit is calculated on a background-only dataset, i.e. without tH contribution, but including a κ_t-dependent contribution from $t\bar{t}H$. The $t\bar{t}H$ normalization is kept fixed in the fit, while the tH signal strength is allowed to float. Limits can be compared to the expected tH cross sections $\times$ branching ratios of 0.834 pb and 0.077 pb for inverted top couplings and for the SM, respectively.

Scenario	Channel	Obs. Limit (pb)	Exp. Limit (pb)
$\kappa_t/\kappa_V = -1$	$b\bar{b}$	6.07	$3.06^{+1.58}_{-0.97}$
	$\gamma\gamma$	1.31	$1.28^{+0.58}_{-0.36}$
	$\mu\mu + e\mu + \ell\ell\ell$	0.87	$0.82^{+0.39}_{-0.25}$
	Combined	**0.86**	$\mathbf{0.59^{+0.26}_{-0.17}}$
$\kappa_t/\kappa_V = 1$ (SM-like)	$b\bar{b}$	8.29	$3.83^{+1.97}_{-1.22}$
	$\gamma\gamma$	5.17	$3.59^{+1.46}_{-0.91}$
	$\mu\mu + e\mu + \ell\ell\ell$	1.40	$1.26^{+0.57}_{-0.37}$
	Combined	**2.04**	$\mathbf{1.04^{+0.43}_{-0.29}}$

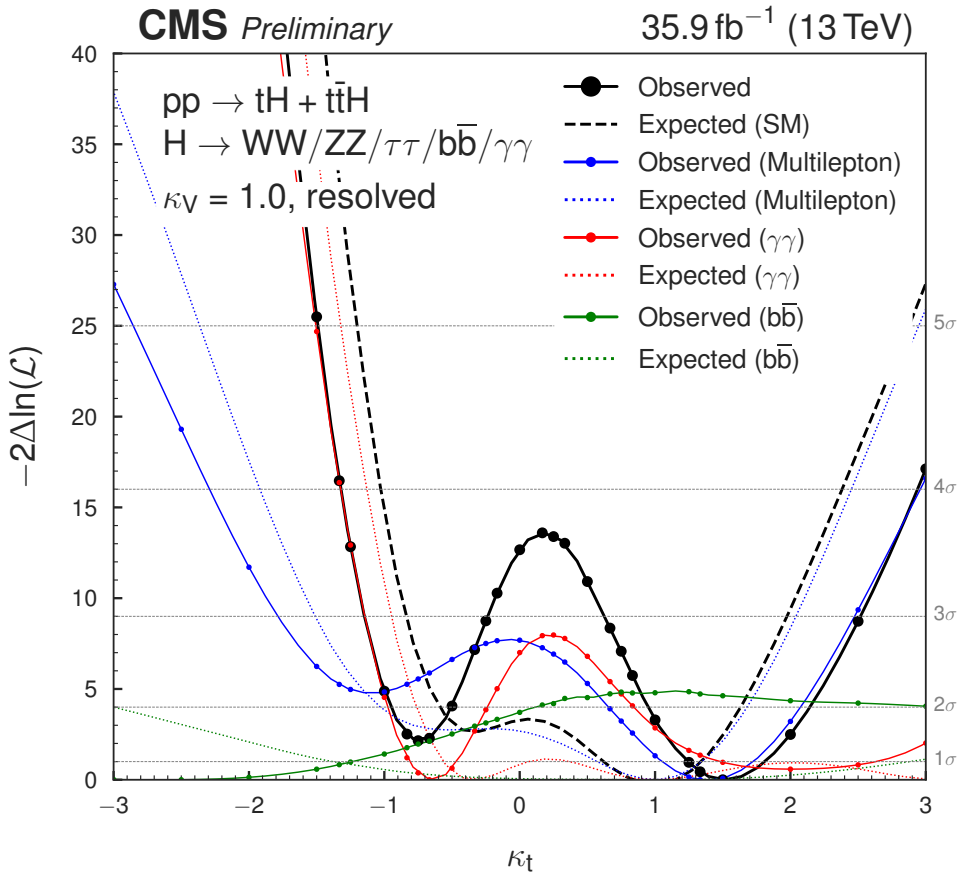

Figure 3: Scan of $-2\Delta\ln(\mathcal{L})$ for the combined fit of the $tH + t\bar{t}H$ signal strength on the data (black line) and the individual channels (blue, red, and green), compared to fits on an Asimov dataset corresponding to the SM expectations (dashed lines). In each point the hypothesis of signal strength equal to one is tested against a fit with floating signal strength. The tH and $t\bar{t}H$ components are varied with a common signal strength.

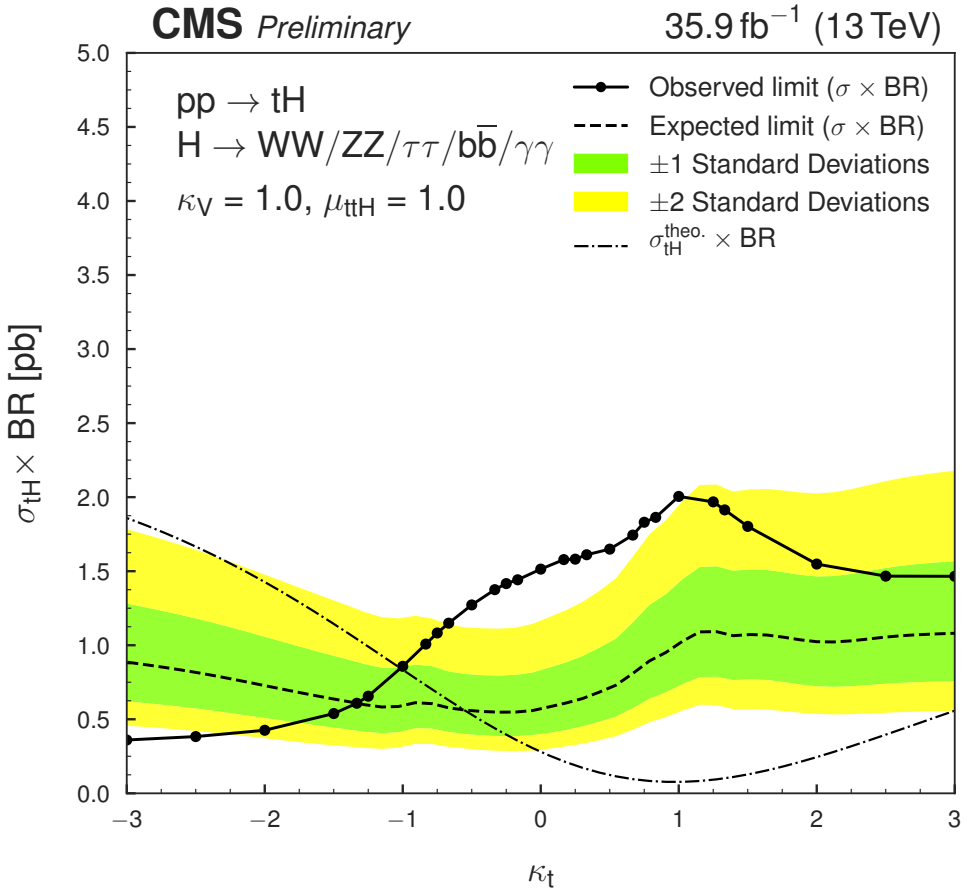

Figure 4: Observed and expected 95% C.L. upper limit on the tH cross section times combined $H \to WW^* + \tau\tau + ZZ^* + b\bar{b} + \gamma\gamma$ branching fraction for different values of the coupling ratio κ_t. The expected limit is calculated on a background-only dataset, i.e. without tH contribution, but including a κ_t-dependent contribution from $t\bar{t}H$. The $t\bar{t}H$ normalization is kept fixed in the fit, while the tH signal strength is allowed to float.

References

[1] ATLAS Collaboration, "Observation of a new particle in the search for the standard model Higgs boson with the ATLAS detector at the LHC", *Phys. Lett. B* **716** (2012) 1, doi:10.1016/j.physletb.2012.08.020, arXiv:1207.7214.

[2] CMS Collaboration, "Observation of a new boson at a mass of 125 GeV with the CMS experiment at the LHC", *Phys. Lett. B* **716** (2012) 30, doi:10.1016/j.physletb.2012.08.021, arXiv:1207.7235.

[3] CMS Collaboration, "Observation of a new boson with mass near 125 GeV in pp collisions at $\sqrt{s}$ = 7 and 8 TeV", *JHEP* **06** (2013) 081, doi:10.1007/JHEP06(2013)081, arXiv:1303.4571.

[4] ATLAS, CMS Collaboration, "Combined Measurement of the Higgs Boson Mass in pp Collisions at $\sqrt{s} = 7$ and 8 TeV with the ATLAS and CMS Experiments", *Phys. Rev. Lett.* **114** (2015) 191803, doi:10.1103/PhysRevLett.114.191803, arXiv:1503.07589.

[5] CMS Collaboration, "Constraints on the spin-parity and anomalous HVV couplings of the Higgs boson in proton collisions at 7 and 8 TeV", *Phys. Rev. D* **92** (2015) 012004, doi:10.1103/PhysRevD.92.012004, arXiv:1411.3441.

[6] CMS Collaboration, "Observation of $t\bar{t}H$ production", *Phys. Rev. Lett.* **120** (2018) 231801, doi:10.1103/PhysRevLett.120.231801, 10.1130/PhysRevLett.120.231801, arXiv:1804.02610.

[7] ATLAS Collaboration, "Observation of Higgs boson production in association with a top quark pair at the LHC with the ATLAS detector", arXiv:1806.00425.

[8] S. Biswas, E. Gabrielli, and B. Mele, "Single top and Higgs associated production as a probe of the Htt coupling sign at the LHC", *JHEP* **01** (2013) 088, doi:10.1007/JHEP01(2013)088, arXiv:1211.0499.

[9] B. Hespel, F. Maltoni, and E. Vryonidou, "Higgs and Z boson associated production via gluon fusion in the SM and the 2HDM", *JHEP* **06** (2015) 065, doi:10.1007/JHEP06(2015)065, arXiv:1503.01656.

[10] J. Ellis and T. You, "Updated Global Analysis of Higgs Couplings", *JHEP* **06** (2013) 103, doi:10.1007/JHEP06(2013)103, arXiv:1303.3879.

[11] CMS Collaboration, "Precise determination of the mass of the Higgs boson and tests of compatibility of its couplings with the standard model predictions using proton collisions at 7 and 8 TeV", *Eur. Phys. J. C* **75** (2015), no. 5, 212, doi:10.1140/epjc/s10052-015-3351-7, arXiv:1412.8662.

[12] ATLAS and CMS Collaborations, "Measurements of the Higgs boson production and decay rates and constraints on its couplings from a combined ATLAS and CMS analysis of the LHC pp collision data at $\sqrt{s} = 7$ and 8 TeV", *JHEP* **08** (2016) 045, doi:10.1007/JHEP08(2016)045, arXiv:1606.02266.

[13] F. Maltoni, K. Paul, T. Stelzer, and S. Willenbrock, "Associated production of Higgs and single top at hadron colliders", *Phys. Rev. D* **64** (2001) 094023, doi:10.1103/PhysRevD.64.094023, arXiv:hep-ph/0106293.

[14] M. Farina et al., "Lifting degeneracies in Higgs couplings using single top production in association with a Higgs boson", *JHEP* **05** (2013) 022, doi:10.1007/JHEP05(2013)022, arXiv:1211.3736.

[15] P. Agrawal, S. Mitra, and A. Shivaji, "Effect of Anomalous Couplings on the Associated Production of a Single Top Quark and a Higgs Boson at the LHC", *JHEP* **12** (2013) 077, doi:10.1007/JHEP12(2013)077, arXiv:1211.4362.

[16] F. Demartin, F. Maltoni, K. Mawatari, and M. Zaro, "Higgs production in association with a single top quark at the LHC", *Eur. Phys. J. C* **75** (2015) 267, doi:10.1140/epjc/s10052-015-3475-9, arXiv:1504.00611.

[17] LHC Higgs Cross Section Working Group Collaboration, "Handbook of LHC Higgs Cross Sections: 4. Deciphering the Nature of the Higgs Sector", doi:10.23731/CYRM-2017-002, arXiv:1610.07922.

[18] CMS Collaboration, "Search for the associated production of a Higgs boson with a single top quark in proton-proton collisions at $\sqrt{s} = 8$ TeV", *JHEP* **06** (2016) 177, doi:10.1007/JHEP06(2016)177, arXiv:1509.08159.

[19] CMS Collaboration, "Search for production of a Higgs boson and a single top quark in multilepton final states in proton collisions at $\sqrt{s} = 13$ TeV", CMS Physics Analysis Summary CMS-PAS-HIG-17-005, CERN, Geneva, 2017.

[20] CMS Collaboration, "Search for the tH($\mathrm{H}\rightarrow \mathrm{b\bar{b}}$) process in pp collisions at $\sqrt{s} = 13\,\text{TeV}$ and study of Higgs boson couplings", CMS Physics Analysis Summary CMS-PAS-HIG-17-016, CERN, Geneva, 2018.

[21] CMS Collaboration, "Measurements of Higgs boson properties in the diphoton decay channel in proton-proton collisions at $\sqrt{s} = 13$ TeV", arXiv:1804.02716. Submitted to JHEP.

[22] CMS Collaboration, "Description and performance of track and primary-vertex reconstruction with the CMS tracker", *JINST* **9** (2014), no. 10, P10009, doi:10.1088/1748-0221/9/10/P10009, arXiv:1405.6569.

[23] CMS Collaboration, "The CMS Experiment at the CERN LHC", *JINST* **3** (2008) S08004, doi:10.1088/1748-0221/3/08/S08004.

[24] CMS Collaboration, "Particle-flow reconstruction and global event description with the CMS detector", *JINST* **12** (2017) P10003, doi:10.1088/1748-0221/12/10/P10003, arXiv:1706.04965.

[25] E. Chabanat and N. Estre, "Deterministic annealing for vertex finding at CMS", in *Computing in high energy physics and nuclear physics. Proceedings, Conference, CHEP'04, Interlaken, Switzerland, September 27-October 1, 2004*, pp. 287–290. 2005.

[26] R. Fruhwirth, W. Waltenberger, and P. Vanlaer, "Adaptive vertex fitting", *J. Phys.* **G34** (2007) N343, doi:10.1088/0954-3899/34/12/N01.

[27] CMS Collaboration, "Performance of Electron Reconstruction and Selection with the CMS Detector in Proton-Proton Collisions at s = 8 TeV", *JINST* **10** (2015), no. 06, P06005, doi:10.1088/1748-0221/10/06/P06005, arXiv:1502.02701.

[28] CMS Collaboration, "Performance of CMS muon reconstruction in pp collision events at $\sqrt{s} = 7$ TeV", *JINST* **7** (2012) P10002, doi:10.1088/1748-0221/7/10/P10002, arXiv:1206.4071.

[29] M. Cacciari, G. P. Salam, and G. Soyez, "The Anti-k(t) jet clustering algorithm", *JHEP* **04** (2008) 063, doi:10.1088/1126-6708/2008/04/063, arXiv:0802.1189.

[30] M. Cacciari, G. P. Salam, and G. Soyez, "FastJet User Manual", *Eur. Phys. J.* **C72** (2012) 1896, doi:10.1140/epjc/s10052-012-1896-2, arXiv:1111.6097.

[31] CMS Collaboration, "Identification of b-quark jets with the CMS experiment", *JINST* **8** (2013) P04013, doi:10.1088/1748-0221/8/04/P04013, arXiv:1211.4462.

[32] CMS Collaboration, "Identification of heavy-flavour jets with the CMS detector in pp collisions at 13 TeV", *JINST* **13** (2018) P05011, doi:10.1088/1748-0221/13/05/P05011, arXiv:1712.07158.

[33] CMS Collaboration, "The CMS trigger system", *JINST* **12** (2017), no. 01, P01020, doi:10.1088/1748-0221/12/01/P01020, arXiv:1609.02366.

[34] J. Allison et al., "GEANT4 developments and applications", *IEEE Trans. Nucl. Sci.* **53** (2006) 270, doi:10.1109/TNS.2006.869826.

[35] J. Alwall et al., "The automated computation of tree-level and next-to-leading order differential cross sections, and their matching to parton shower simulations", *JHEP* **07** (2014) 079, doi:10.1007/JHEP07(2014)079, arXiv:1405.0301.

[36] NNPDF Collaboration, "Parton distributions for the LHC Run II", *JHEP* **04** (2015) 040, doi:10.1007/JHEP04(2015)040, arXiv:1410.8849.

[37] LHC Higgs Cross Section Working Group Collaboration, "Handbook of LHC Higgs Cross Sections: 3. Higgs Properties", doi:10.5170/CERN-2013-004, arXiv:1307.1347.

[38] F. Demartin et al., "tWH associated production at the LHC", *Eur. Phys. J.* **C77** (2017) 34, doi:10.1140/epjc/s10052-017-4601-7, arXiv:1607.05862.

[39] P. Nason, "A New method for combining NLO QCD with shower Monte Carlo algorithms", *JHEP* **0411** (2004) 040, doi:10.1088/1126-6708/2004/11/040, arXiv:hep-ph/0409146.

[40] S. Frixione, P. Nason, and C. Oleari, "Matching NLO QCD computations with parton shower simulations: the POWHEG method", *JHEP* **11** (2007) 070, doi:10.1088/1126-6708/2007/11/070, arXiv:0709.2092.

[41] S. Alioli, P. Nason, C. Oleari, and E. Re, "A general framework for implementing NLO calculations in shower Monte Carlo programs: the POWHEG BOX", *JHEP* **06** (2010) 043, doi:10.1007/JHEP06(2010)043, arXiv:1002.2581.

[42] E. Re, "Single-top Wt-channel production matched with parton showers using the POWHEG method", *Eur. Phys. J.* **C71** (2011) 1547, doi:10.1140/epjc/s10052-011-1547-z, arXiv:1009.2450.

[43] S. Alioli, P. Nason, C. Oleari, and E. Re, "NLO single-top production matched with shower in POWHEG: s- and t-channel contributions", *JHEP* **0909** (2009) 111, doi:10.1007/JHEP02(2010)011, 10.1088/1126-6708/2009/09/111, arXiv:0907.4076.

[44] T. Melia, P. Nason, R. Rontsch, and G. Zanderighi, "W^+W^-, WZ and ZZ production in the POWHEG BOX", *JHEP* **1111** (2011) 078, doi:10.1007/JHEP11(2011)078, arXiv:1107.5051.

[45] T. Sjöstrand et al., "An Introduction to PYTHIA 8.2", *Comput. Phys. Commun.* **191** (2015) 159–177, doi:10.1016/j.cpc.2015.01.024, arXiv:1410.3012.

[46] CMS Collaboration, "Evidence for associated production of a Higgs boson with a top quark pair in final states with electrons, muons, and hadronically decaying τ leptons at $\sqrt{s} = 13$ TeV", arXiv:1803.05485. Submitted to JHEP.

[47] CMS Collaboration, "Search for $t\bar{t}H$ production in the $Hb\bar{b}$ decay channel with leptonic $t\bar{t}$ decays in proton-proton collisions at $\sqrt{s} = 13$ TeV", (2018). arXiv:1804.03682. Submitted to *JHEP*.

[48] P. Dauncey, M. Kenzie, N. Wardle, and G. Davies, "Handling uncertainties in background shapes: the discrete profiling method", *JINST* **10** (2015) P04015, doi:10.1088/1748-0221/10/04/P04015.

[49] CMS Collaboration, "Observation of the diphoton decay of the Higgs boson and measurement of its properties", *Eur. Phys. J.* **C74** (2014), no. 10, 3076, doi:10.1140/epjc/s10052-014-3076-z, arXiv:1407.0558.